Surface structuring by Electron Beam for improved soft tissues adhesion and reduced bacterial contamination on Ti-grade 2

Surface structuring by Electron Beam for improved soft tissues adhesion and reduced bacterial contamination on Ti-grade 2

S. Ferraris[1], F. Warchomicka[2], C. Ramskogler[2], M. Tortello[1], A. Cochis[3], A. Scalia[3], G. Gautier di Confiengo[4], J. Keckes[5], L. Rimondini[3], S. Spriano[1]

[1] Department of Applied Science and Technology, Politecnico di Torino, TORINO, Italy

[2] Institute of Materials Science, Joining and Forming, Graz University of Technology, GRAZ, Austria

[3] Department of Health Sciences, Università del Piemonte Orientale, NOVARA, Italy

[4] CNR-IMAMOTER, TORINO, Italy

[5.] Department of Materials Physics, Montanuniversität Leoben and Erich Schmid Institute for Materials Science, Austrian Academy of Sciences, Leoben, Austria

Corresponding Author:

Sara Ferraris

Department of Applied Science and Technology

Politecnico di Torino, Corso Duca degli Abruzzi 24, 10129 Turin (TO), Italy

sara.ferraris@polito.it

Abstract

Even if soft tissue adhesion on titanium surfaces is an issue of great interest for transmucosal dental implants and percutaneous devices, few specific surface modification strategies have been approached so far to face it. Topographical surface modification is an interesting strategy because quality of soft tissues can be effectively improved by contact guidance effect on fibroblasts. Conversely, biofilm formation is encouraged in presence of rough or porous surfaces, as well as of surface patterns, if the roughness overcome the threshold of 0.2 µm. This issue becomes particularly critical in medical devices which cross different biological tissues and, through soft tissues, establish a direct contact with the external environment. In the present research, three different grooved patterns (5, 10 and 30 micron wide) were produced on commercially pure titanium by means of Electron Beam (EB) structuring maintaining the average surface roughness lower than 0.2 µm. The EB surface structured samples were characterized by means of optical and atomic force microscopy, contact and non-contact profilometry, X-Ray Diffraction, residual stress measurements as well as bacteria and cell adhesion tests. The 10 µm wide grooves resulted able to support fibroblast alignment onto the metallic substrate. Unexpectedly, all the EB surface structured surfaces not only did not enhance, but even reduced bacterial adhesion up to 48h culture.

Graphical Abstract

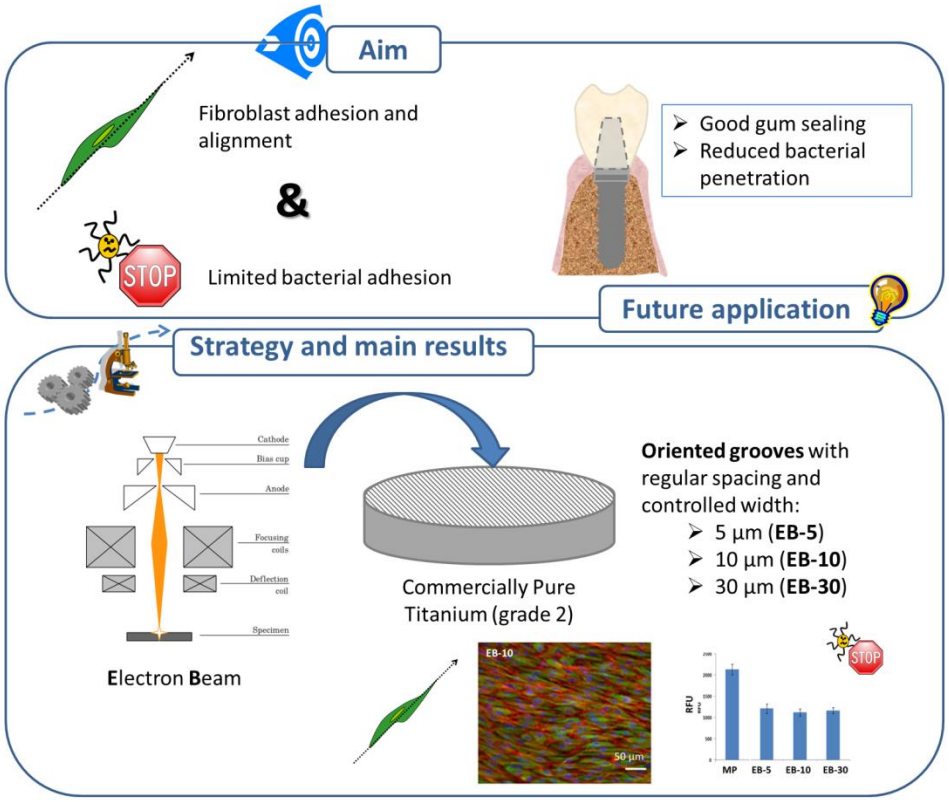

Keywords: Electron Beam; Titanium; Surface Structuring; Oriented Grooves; Fibroblast Alignment; Bacterial Adhesion

1. Introduction

Surface topographical features significantly affect adhesion and behavior of both cells and bacteria even if in different ways, as explained by Jaeger and Brunette (2001) for microfabricated surfaces or by Brunette (2001) for machined ones. Bacteria are typically 1-2 µm in size, cells like fibroblasts and osteoblasts are comprised between 15 and 25 µm, so different micro scaled topographies differently affect them. Moreover, while bacteria have a rigid structure, cells can modify their shape in order to follow surface topography during adhesion and focal contacts formation. Considering that different cells and bacteria differ by dimensions, rigidity and specific features, not all cells/bacteria species will be affected at the same manner by the same surface pattern, as suggested by Anselme et al (2010). Different cell types preferentially adhere to specific topographies. Osteoblasts are generally rugophilic (preferentially adhere to rough surfaces) as well as bacteria, which adhesion is significantly enhanced on rough surfaces; a threshold value of the surface roughness (0.2 µm) has been reported in literature as the lower limit below which bacterial adhesion does not increase, as observed in *in vitro* tests by Frijd et al (2011), in *in vivo* evaluations by Al-Ahmad (2013) or in clinical tests by Quirynen et al. (1996) . On the other hand, fibroblasts are rugophobic (preferentially adhere to smooth surfaces), but they are sensitive to surface patterns and in particular they align onto surface micro/nano grooves by means of the contact guidance phenomenon, widely described in literature (Brunette 2001).

The present research is focused on titanium surfaces aimed at supporting soft tissues and discouraging bacterial contamination/penetration, as requested in the collar region of transmucosal dental implants and in percutaneous devices. Taking into account the data reported in literature collected and compared by Spriano and Ferraris (2014) and obtained by the authors themselves (Ferraris et al 2017), the following rationale was followed in order to design the surface pattern: average surface roughness (Ra) lower than 0.2 µm, in order to avoid an increment of bacteria adhesion, and grooves with width higher than 100 nm and lower than 70 µm, depth higher than 35 nm and with spacing between grooves lower than 2 µm in order to get contact guidance effect on fibroblasts. In a previous work, the authors obtained similar grooves by an optimized protocol of polishing by abrasive papers and demonstrated the ability of the properly polished surfaces to favor fibroblast alignment without increasing bacterial adhesion (Ferraris et al 2017). Considering that mechanical polishing does not allow a control on width and spacing of the grooves, an alternative technology was proposed here.

Numerous technological strategies are suitable for obtaining micro and nano-patterns on titanium surfaces, such as Photolithography (Liu and Jay 2007), Ion Milling, Chemical Etching, Micromachining (Lu and Leng 2005) Jet Electrochemical Machining (Madore et al 1999), Focused Ion Beam (FIB), Electron Beam Lithography, Laser Structuring with pulsed lasers, Plasma Etching, Ion etching and Printing. (Etheridge et al). The use of a highly energetic electron beam (EB) technique was selected. Its advantages include the possibility to get a wide variety of structures at the microscale level in metals and a fast repeatable process under vacuum. The process has similar principle to the conventional scanning electron microscope, where a high-speed focused electron beam impact against the material and it causes melting, local evaporation and a keyhole effect, as describes by Schulz (2004). The deflection of the EB can be programmed to generate specifically designed patterns on metallic materials. Dance et al. (2007) developed the Surfi-Sculpt® technology based on the effect of creating protrusion patterns by repeating the beam movement on the same path, for a wide field of applications. Recently, Ramskogler et al (2017) obtained multi scale topography by EB in Ti6Al4V and showed successfully results for biomedical applications, with a homogeneous spreading and polygonal morphology of MC3T3-E1 pre-osteoblastic cells after different cultivation times.

In the present paper, Electron Beam (EB) structuring has been applied to Ti-cp samples in order to obtain a parallel periodic oriented groove pattern with nominal grooves' width of 5 µm, 10 µm and 30 µm (EB- 5, EB – 10 and EB – 30 respectively) and an average surface roughness lower than 0.2 µm in order to induce fibroblast alignment without increasing bacterial adhesion. The EB surface structured samples have been characterized by means of optical microscopy, Atomic Force Microscopy (AFM) contact and optical profiler for the investigation of surface topography and roughness, X-ray diffraction for the analysis of crystallographic structure and residual stresses. Cellular and bacterial adhesion tests were performed to evaluate the biological response to the EB surface structured samples in comparison with mirror polished and/or mechanically structured surfaces by controlled polishing with abrasive papers.

Despite numerous studies have been reported on fibroblasts response to micro and nano-structured surfaces, as previously discussed by the authors (Spriano and Ferraris 2014, Ferraris et al 2017), few researches consider dental implants as application field and almost no research work or patent considers surface modification of titanium in order to simultaneously obtain fibroblast attachment and orientation, as well as reduced bacterial adhesion. Accordingly, the present paper describes for the first time the use of Electron Beam for the obtainment of grooved titanium surfaces able to support fibroblast adhesion and alignment and to limit bacterial contamination. Moreover, for the first time the influence of microstructure on bacterial adhesion has been demonstrated on microstructured titanium surfaces. The here produced surfaces are of interest in the production of innovative dental implants collars.

2. Materials and methods

2.1 Samples preparation

Commercially pure titanium (Ti-c.p. - ASTM B348, Gr2, Titanium Consulting and Trading) plane samples (2 mm thick and 10 mm in diameter) were used as substrates.

Surface structuring was performed by an electron beam (EB) machine, model Probeam EBG 45-150 K14. Before structuring, the samples were mirror polished with SiC abrasive papers (up to 4000 grit). At the end of the polishing process, the samples were washed in ethanol for 5 min in an ultrasonic bath. The chamber of the EB welding machine was under vacuum during all the experiments. The setup to produce surface geometries included as first the adjustment of the energy input, denoted by beam voltage, beam current and beam velocity. The EB machine offers a faster beam deflection due to the guiding of electrons by the magnetic field without inertia and very precisely positioning, giving a maximum beam deflection in this machine up to 200mm in both X and Y axes. For this reason, samples were fixed at the stage for a precise structuring. The beam focus was kept constant at the surface of the material. Then, the generation of a basic structure geometry occurred by coordinate points. The structure consists of parallel lines, where the nominal groove width varied between 5 µm, 10 µm and 30 µm. Due to the size of the beam focused on the surface of the substrate, about 280µm, a strategy of overlapping of single electron beam beads were carried out to produce the nominal groove width. Numerical control program was used to control the beam deflection of the figure (line) by giving the coordinates for initial and end position of each line and the beam velocity. In order to produce an homogenous pattern on the surface, deflection figures (swipe) was repeated several times depending on the beam velocity.In this work, the electron beam was displacing

continuously on the surface of the substrate, without pitch strategy as usually used by laser structuring technique.

The sizing (area) of the structure was set by programming the X and Y amplitudes in the EB machine. In this work, an area of 7 x 7 mm^2 was performed for all the investigations. Figure 1 shows a schematic illustration of an electron beam principle and the beam technique for structuring proposed in this work. Table 1 summarizes the parameters used for EB surface structuring.

Table 1. Parameters to produce surface geometries

energy input			Number of swipes	nominal groove width [µm]
voltage [kV]	current [mA]	Beam velocity [mm/s]		
150	0.8	853	2	30
150	0.8	3333	3	10
150	0.8	5333	3	5

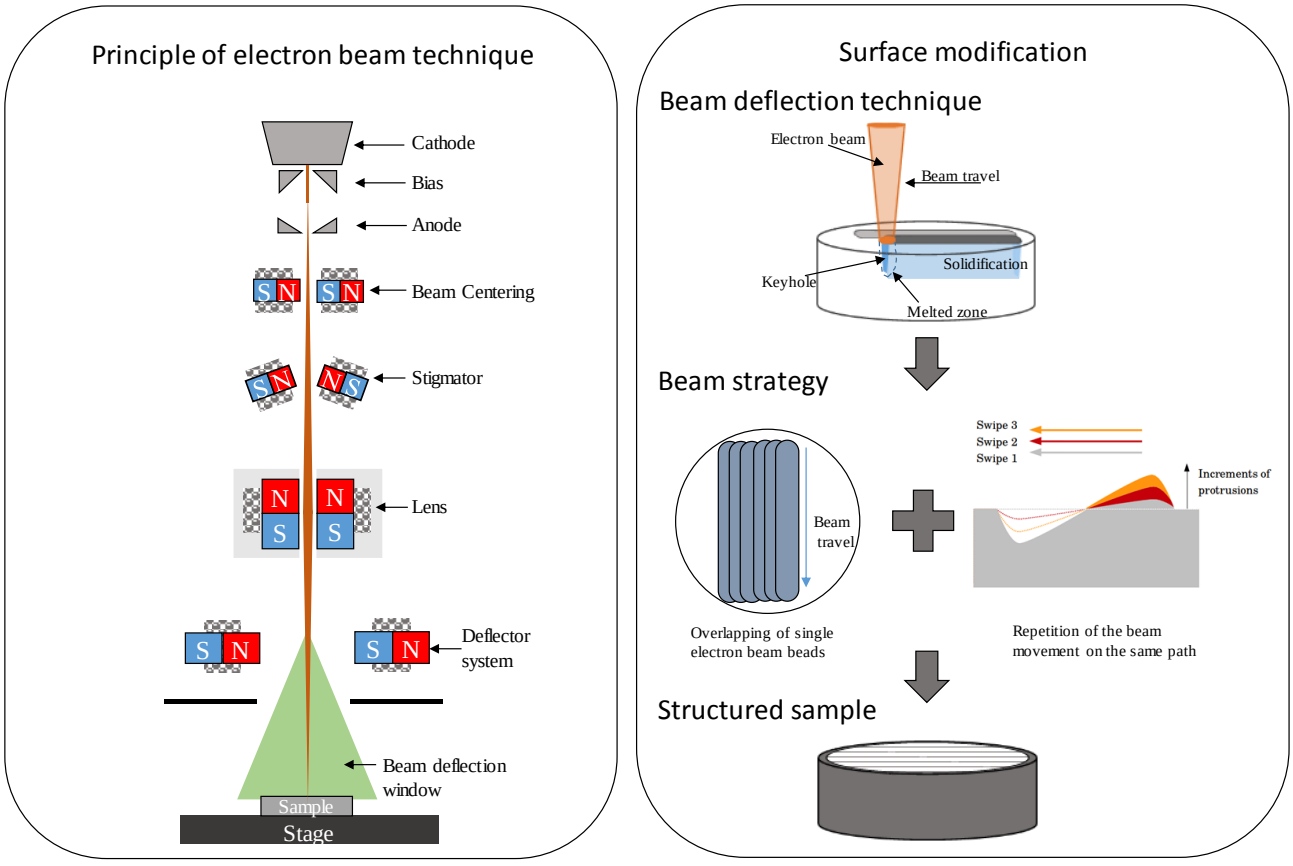

Figure 1: Schematic illustration of an electron beam principle (based on Adam et al (2011)) and the surface modification technique proposed in this work.

After EB surface structuring, the samples were washed again once in acetone (for 5 min) and twice in ultrapure water (for 10 min) in an ultrasonic bath. The EB surface structured samples were named accordingly to the nominal groove width, such as EB-5 (grooves 5 micron wide), EB-10 (grooves 10 micron wide) and EB-30 (grooves 30 micron wide).

As reference, mechanically structured samples obtained by using abrasive papers (AP samples) were prepared according to a protocol of controlled polishing previously described by the authors (Ferraris et al 2017). Mirror polished samples were used as reference as well.

2.2 Physico-chemical characterization

Surface topographies were investigated with a light optical microscope (ZEISS observer.Z1m) equipped with an AxioCam MRc5. Pictures of the structured surfaces were taken by polarized light and with an Atomic Force Microscope (AFM, - Innova, Bruker). The AFM measurements were performed in the contact mode and the topography maps were analyzed by means of the Gwyddion software.

Surface roughness was measured by means of a contact profiler (Talysurf 120), moreover the surface 3D reconstruction was performed on all the samples by means of an optical profiler (Talysurf CCI3000Å; ×50 objective).

Crystalline structure of the grooved samples was investigated by means of X-Ray Diffraction (XRD, PANalytical X'Pert Pro PW 3040160 Philips) and compared with the data obtained on the mechanically roughened samples. XRD spectra were analyzed by means of XPERT High Score software.

XRD residual stress characterization was performed using a Rigaku SmartLab 5-axis diffractometer equipped with Cu-Kα radiation, a primary parabolic multilayer mirror, a secondary graphite monochromator and a scintillation detector. The residual stress were characterized using $\sin^2\psi$ method (Noyan and Cohen 1987) by performing diffraction scans at Ti 101 reflections in the 2θ range of 38.5-41.5 degrees and in the ψ range of 0-56.7degree using a measurement step of 0.02 deg and a speed of 2 deg/min. X-ray elastic strains were determined at eight sample tilt angles and along two perpendicular diffraction vector tilt planes. This allowed to evaluate biaxial residuals stresses along two perpendicular in-planes sample directions A and B by using X-ray elastic constant 0.5 s2= 1.1791 10^{-11} Pa^{-1} of Ti 101 reflection. In this way, it was possible to evaluate stress components oriented parallel (A) and perpendicular (B) to the groove direction.

Hardness measurements were carried out using a EMCO Test (M10 010) with an indentation load of 0.1 kg (HV 0.1) and a dwell time of 15 s. Six to eight indentations were taken in the base material and at the EB structured close to the surface and the average value was calculated to determine the changes on the mechanical properties.

2.3 Cytocompatibility and cell orientation

The samples were sterilized for 2h at 180°C prior to use with cells. Then, they were handled with sterile tweezers by lateral side in order to avoid any surface damage.

2.3.1 Cells

In vitro cytocompatibility evaluation was performed using gingival human primary fibroblasts (HGFs). Primary cells were enzymatically isolated from discarded healthy human gingiva specimens obtained after surgical resection. All practices were performed after Patient's informed consent approval and in full compliance with the Helsinki Declaration. HGFs were obtained by digesting the gingiva epithelial layer with a solution of collagenase/dispase/trypsin (1 mg mL^{-1} collagenase, 0.3 mg mL^{-1} dispase, 0.25% trypsin in PBS, Sigma) for 30 minutes at 37°C. After digestion, isolated cells were collected and cultivated with complete

medium made of Minimal Essential Medium alpha-modification (a-MEM, from Sigma), 10% foetal bovine serum (FBS, Lonza) and 1 % antibiotics. Cells were maintained at 37°C, 5% CO_2 atmosphere and used between passages 2-4 to prevent spontaneous immortalization.

2.3.2 In vitro Direct Cytocompatibility

Test specimens were individually placed into the wells of 24-multiwell plate; then, a defined number of HGFs ($2x10^4$ cells/specimen) were dropwise spotted directly onto specimens' surface, thus allowing a direct contact between cells and specimens. Afterwards, each well was rinsed with 1 ml of complete medium and cells were cultivated for 48 h at 37°C, 5% CO_2. Cells cultivated onto mirror-polished specimens were considered as control. Finally, cells viability was determined by the metabolic colorimetric alamar blue assay (alamarBlue, Thermo-Scientific); briefly, medium was removed from each well and replaced with 1 ml of alamar blue solution (0.25% in PBS). Plate was incubated 4 h in the dark at 37°C; then, 200 ml were collected from each specimen and transferred to a 96 wells plate for evaluation. Optical density (o.d.) was measured using a 590 nm wavelength by means of spectrophotometer (Victor, Perkin Elmer).

2.3.3 In vitro Indirect Cytocompatibility

For the indirect assay, a pre-conditioned medium was used to cultivate cells in order to evaluate the release of any toxic compounds from the specimens. Accordingly, specimens were submerged with serum-free basal medium (a-MEM, 1 ml / specimens) for 7 days; then, eluates were harvested, added of 10% FBS and 1% antibiotics to obtain a complete medium and used to cultivate HGFs for 48 h ($2x10^4$ cells / well into a 24-multiwell plate). Cells cultivated with fresh complete medium were used as control. Finally, cells viability was evaluated by the alamar blue assay as prior detailed in 2.3.2.

2.3.4 Morphology

At the end of the direct assay, cells morphology was visually investigated by means of field emission scanning electron microscopy (FESEM) and immunofluorescence (IF) staining.

For FESEM analysis, specimens were fixed with 3% paraformaldehyde for 2h at room temperature (RT), dehydrated by alcohol scale (70-80-90-100 % ethanol, 10 minutes each, from Sigma), swelled with examethildisilazane (2 minutes, from Sigma) and air dried under the laminar hood flow. Finally, specimens were gently fixed onto stubs by conductive carbon tape, covered with a chromium layer and visually checked by FESEM (SUPRATM 40, Zeiss) using different magnifications.

For IF staining, cells were fixed 20 minutes with 3% paraformaldehyde RT, washed with PBS and stained with an anti-vimentin (AbCam, 1:150 in PBS, 5% goat serum, 1% BSA) and anti-collagen type II (AbCam, 1:100 in PBS, 5% goat serum, 1% BSA) for 1h, RT. Afterwards, the excess was washed out by PBS prior to add an appropriate secondary antibody (45 minutes, RT); finally, cells were co-stained with phalloidin (AbCam, 1:500 in PBS) and 4,6-diamidino-2-phenylindole (DAPI, Sigma) to visualize cytoskeleton f-actins and nuclei. Images were acquired by fluorescent microscope (Leica 6500, Leica Microsystems).

A software of image analysis (Digimizer 4.3.0)was employed for the evaluation of cell alignment . The angle between the main axis of a cell and the grooves direction (or the horizontal axis where no groove was present) was measured. For each type of sample at least 50 measurements were performed on the images obtained through the fluorescent microscope (phalloidin).

2.4 Bacterial adhesion

2.4.1 Bacteria growth conditions

A clinical isolate, multi-drug resistant (mdr) verified strain of *Staphylococcus aureus* (*S. aureus*) was obtained from the Clinical Microbiology Unit at the Maggiore Hospital in Novara after obtaining Patient's signed informed consent. Bacteria were isolated and selected by using selective Mannitol Salt agar plates (from Sigma) until round shaped yellow colonies were obtained. Fresh broth culture was arranged prior to each experiment by melting 3 colonies into 30 ml of Luria-Bertani broth (LB, from Sigma) at 37°C, 200 rpm shacking overnight to induce bacteria exponential growth phase. Finally, broth culture was diluted until the final density of $1x10^7$ cells / ml according to the o.d. at 600 nm (corresponding to 0.001).

2.4.2 Bacterial adhesion evaluation

To test surface anti-adhesion properties, specimens were seeded onto a 24-multiwell plate and submerged with 1 ml of the $1x10^7$ cells / ml bacteria suspension obtained as detailed in 2.4.1. Bacteria were allowed to adhere for 2h (at 37°C); then, the biomass viability was evaluated alamar blue assay, while the viable bacteria number by the colonies forming units (CFU) count. Alamar blue assay was performed as prior detailed in 2.3.2, while for CFU count adhered bacteria were detached by vortex and sonication (30 sec each, 3 times) and collected into sterile PBS. Then, 100 µl were collected and 1:10 diluted 6 times with fresh PBS. From each of the six ten-folder dilutions, 20 µl were collected and spotted onto LB agar plates that were stored at 37°C for 24 h. Once single defined round colonies were formed, the total number of CFUs were counted as follow:

CFU number = [(n. colonies x dilution factor) x 10^(serial dilution)]

The bacteria cultivated onto mirror polished titanium were used as control.

2.4.3 Biofilm biomass viability

To test specimens' ability to prevent surface biofilm formation, they were infected for 24-48-72 h with a $1x10^7$ cells / ml bacteria suspension obtained as detailed in 2.4.1. Specimens were submerged with 1 ml and incubated for 90 min at 37°C in agitation (200 rpm) in order to force biofilm cells adhesion (adhesion phase); then, the supernatants were removed to eradicate planktonic cells and replaced with fresh LB medium to grow biofilm (separation phase) for 24-48-72 h. Biofilm biomass viability and number were evaluated by the alamar blue and CFU count assays as prior described, respectively. The bacteria cultivated onto mirror polished titanium were used as control.

2.5 Statistical analysis of the data

Experiments were performed in triplicate. Data were collected and statistically surveyed by the Statistical Package for Social Sciences (SPSS v20.0, IBM). Prior to apply analysis, the Leven's test was used to verify data homogeneity while errors normal distribution was checked by Kolmogorov–Smirnov tests. Finally,

results were analysed by analysis of variance one-way ANOVA and post hoc Sheffe's test; 5% was assumed as significant level.

3. Results and discussion

3.1 Physico-chemical characterization

Microstructure and topography of the EB grooved samples were investigated by optical microscopy and the obtained images are reported in Figure 2. As reference, the images of a mechanically roughened (Figure 2a) and mirror polished (Figure 2b) samples are reported in the same Figure. The surface of the EB grooved samples (Figure 2c, d, e) did not show any imperfection related to the process, such as pores, cracks or rest of material after electron beam structuring, but zones with massive martensite were observed on all the samples. This effect can be related to the thermal stresses generated during fast cooling (Lutjering and Williams 2003) and presence of impurities (Gu et al 2012) that could retard the diffusional transformation from β to α phase (Oh et al 2004) . Good reproducibility of the surface patterns was observed mainly for the samples with 10 and 30µm wide grooves (Figure 1 d and e) for the whole area, while in the case of EB5 the grooves are discontinued in several areas. The beam strategy used in this work showed a good accuracy in the production of the grooves, with a maximum difference of about 10% between the actually achieved and nominal dimensions. A good alignment of the grooves obtained by the developed protocol of mechanical roughening can be observed in Figure 1a even if, obviously, in the case of a mechanically structured surface, width and spacing of the grooves is not controlled: this topography will be used as reference, in order to evaluate the biological effect of a greater control on the geometry of the surface pattern.

During EB surface structuring, the heat input formed a gradient of microstructure, which can be as observed in Figure 2f for the sample structured by 30µm grooves. Three main zones can be characterized: α lath grains and coarser alpha grains located near to the surface and very fine grains in the substrate reproducing the as received microstructure. Surface structuring by electron beam proceeded a complete melting and solidification due to high heating and cooling rates reached by the high-energy beam. It leads to non-equilibrium solidification with formation of α' martensite and α lath phases (see below the XRD data), depending on the energy and the beam velocity (Table 1). The increment of the electron beam velocity directly affected undercooling in the molten pool, favoring formation of α' martensite. Thermal conductivity and the number of swipes helped to coarse microstructure during EB surface structuring. The depth affected by the electron beam was around 120µm (molten zone), while the transition between the molten zone and the heat affected zone (below it) is almost negligible. The hardness of the substrate near to the surface changed after the processing. In the molten zone the hardness was 189 HV0.1 ± 22, while the base material had a hardness value of 164 HV0.1 ± 11. The strengthening of the molten zone were related mainly to: a) the morphology of the alpha grains (alpha laths) due to the fast cooling close to the surface, b) substructure formation by a non-equilibrium phase transformation (Palanivel et al 2017, Liu et al 2012) and c) the thermal stresses related to the process (see below residual stresses measurements). Coarser grains were not affecting the hardness values in comparison with the other factors.

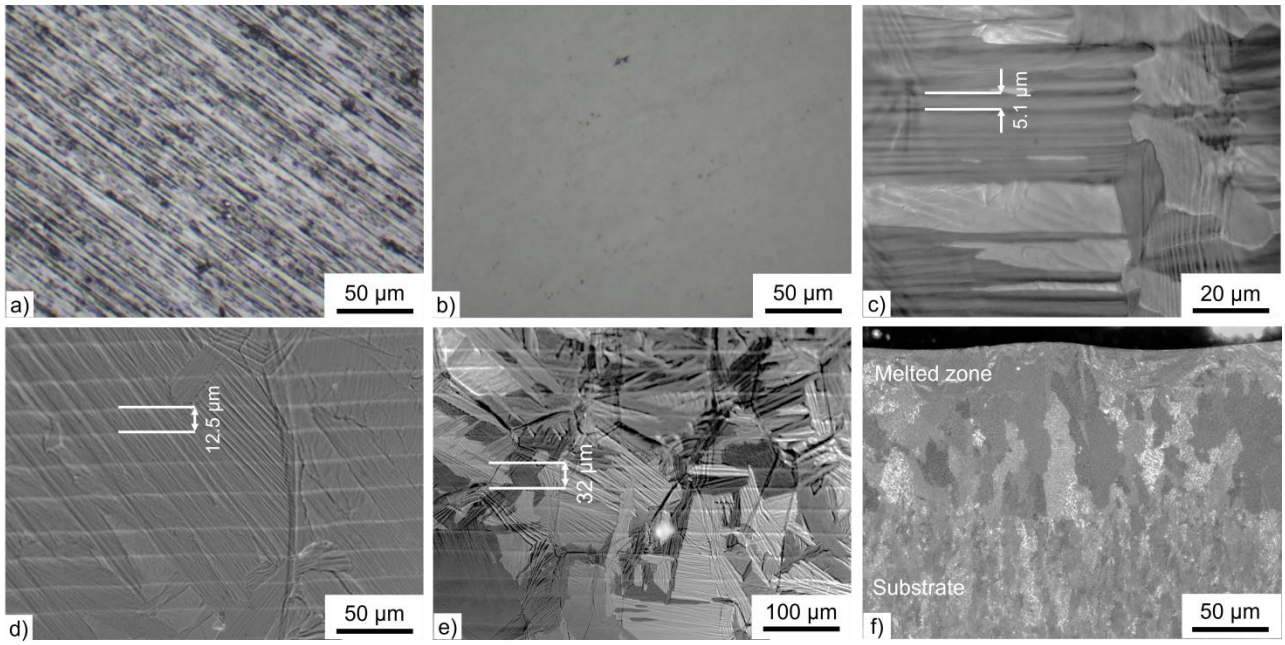

Figure 2: Optical images with polarized light of: a) surface of the mechanically structured sample (AP); b) surface of the mirror polished substrate; c) surface after EB structuring with 5µm wide grooves (EB-5); d) surface after EB structuring with 10µm wide grooves (EB-10); e) surface after EB structuring with 30µm wide grooves (EB-30) and f) cross section of the sample EB-30

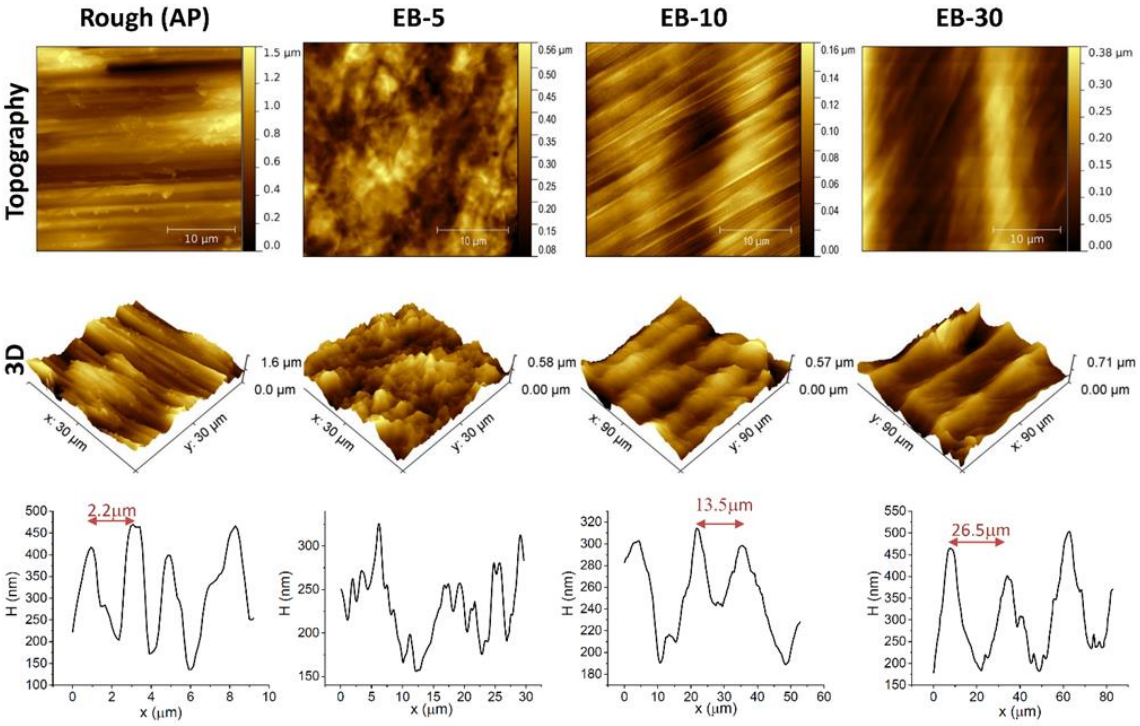

Figure 3: AFM observations on the EB grooved and mechanically roughened samples together with examples of line profiles

Figure 3 shows the topography maps of the EB structured samples along with their 3D visualization. Images of a mechanically structured sample are reported for comparison.

In the case of the AP sample, the grooves are regularly developed, almost parallel, with a width (peak to peak distance) around 1-2.5 µm and sharp edges between valleys (spacing between the edges of two bordering grooves is less than 1 µm wide); some defects can be evidenced as protruding peaks. As far as the EB-5 sample is concerned, it was not possible to individuate the 5 µm wide grooves in the AFM topographic signal, while on the other hand they were clearly visible on both the EB-10 and EB- 30 samples. On these samples, the grooves are regular in shape and almost free from defects as already observed on a larger area by optical microscopy. Scanning perpendicularly to the grooves was more effective in evidencing them, because every single line of scan records the surface topography and the instrumental noise or the possible tiny mechanical adjustments of the probe are minimized along the scan direction rather than between adjacent lines. The peak to peak distance (groove width) is about 12.0-18.0 µm or 25.0-28.0 µm in the case of respectively the EB10 and EB30 samples. The peak to peak distance is about 1-2 µm in the case of the AP sample and the top edges between the grooves are submicrometric in width. The peak to valley distance for the structured grooves in the EB-10 sample is on average about 80-150 nm, while for the EB-30 one is slightly larger, i.e. 200-300 nm. In the case of the AP sample, the average peak to valley distance is 200-350 nm if we consider an area without any evident protruding defect, while it can reach 1.1 µm if we consider a large area including defects. These results, confirm that the samples have surface patterns with dimensions (depth and width of the grooves, spacing between grooves) falling within the limits reported in literature for contact guidance effect and absence of an increment of bacteria adhesion (Spriano and Ferraris 2014), as suggested by the rationale of the research and by previous data of the author (Ferraris et al 2017). As expected, mechanically and EB structured surfaces differ for the defect density (higher in the case of AP), width of the grooves and spacing between bordering grooves: the grooves are narrower and spaced through sharper top edges in the case of AP.

Surface roughness R_a was measured on all the samples by means of a contact profiler while the surface 3D reconstruction has been performed on all the samples by means of an optical profiler. Results are reported in Figure 4.

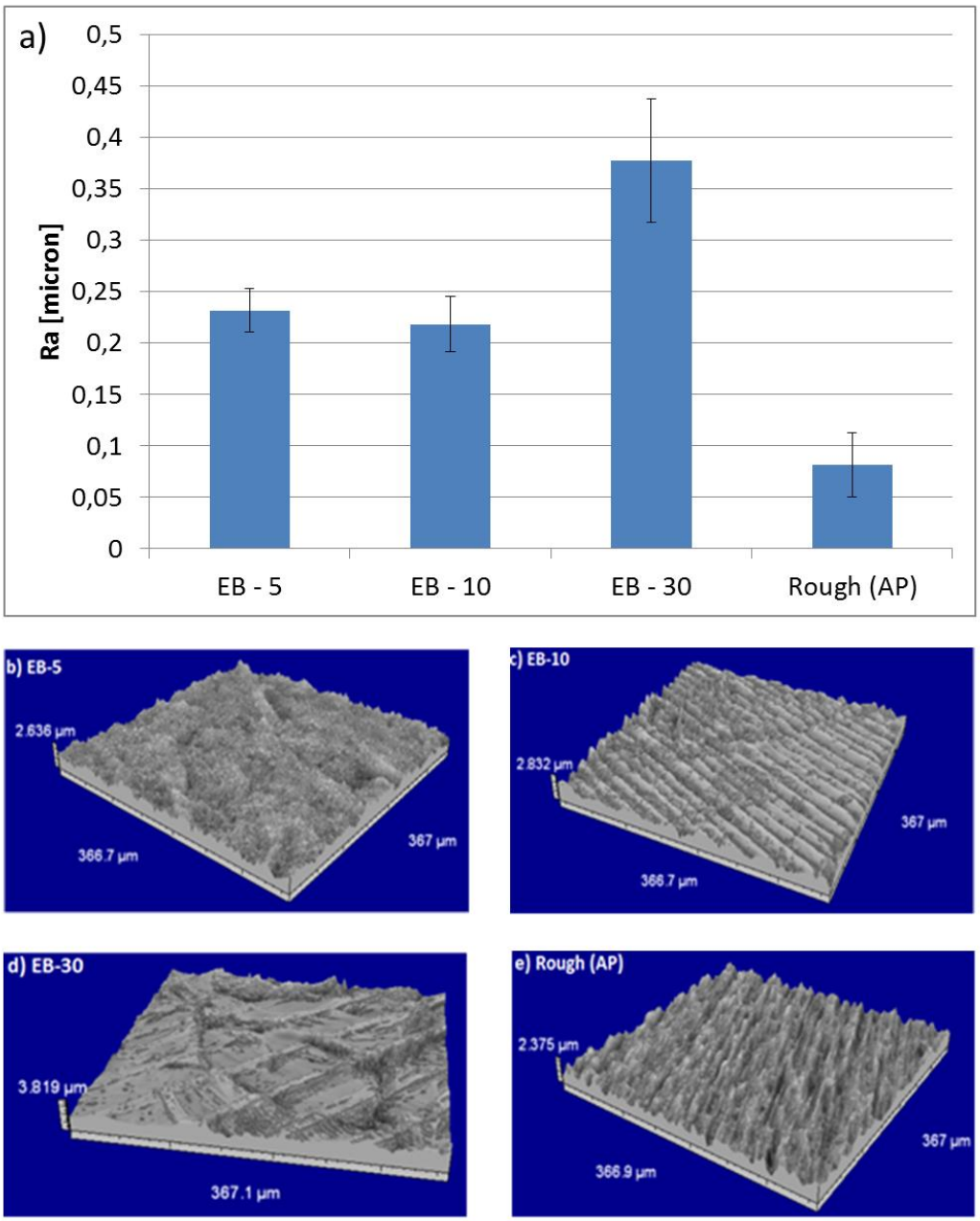

Figure 4: Roughness measurements and surface 3D reconstructions of the EB structured and mechanically roughened samples (AP)

Roughness measurements by contact profilometry (Figure 4a) are in accordance with peak to valley estimation by AFM reported above. Roughness of the EB samples is higher than what measured on the AP sample ($p<0.05$). The Ra values obtained on the AP, EB5 and EB10 samples are lower or close to the threshold value reported for avoiding an increased surface bacterial contamination (0.2 µm) in *in vitro* (Frijd et al 2011), *in vivo* (Al-Ahmad et al 2013) or during clinical tests (Quirynen et al 1996), while EB30 is slightly above it.

Looking at the 3D reconstruction images (Figure 4 b-d) the oriented grooves are not visible on the EB5 sample, while they are visible on the EB10 sample and regular and evident on the EB30 one. These results

are in accordance with the AFM ones. Irregular and very rough areas are observable on all the EB surface structured samples, but they are progressively less evident moving from EB5 (where they cover almost all the surface and grooves are no observable) to EB10 and EB30. According to optical observation of microstructure and to crystallographic data (see below XRD section), the irregular rough areas can be related to martensite grains. As expected, the grooves on the mechanically structured samples are well oriented and irregularly spaced.

XRD spectra have been acquired on all the samples and they are reported in Figure 5.

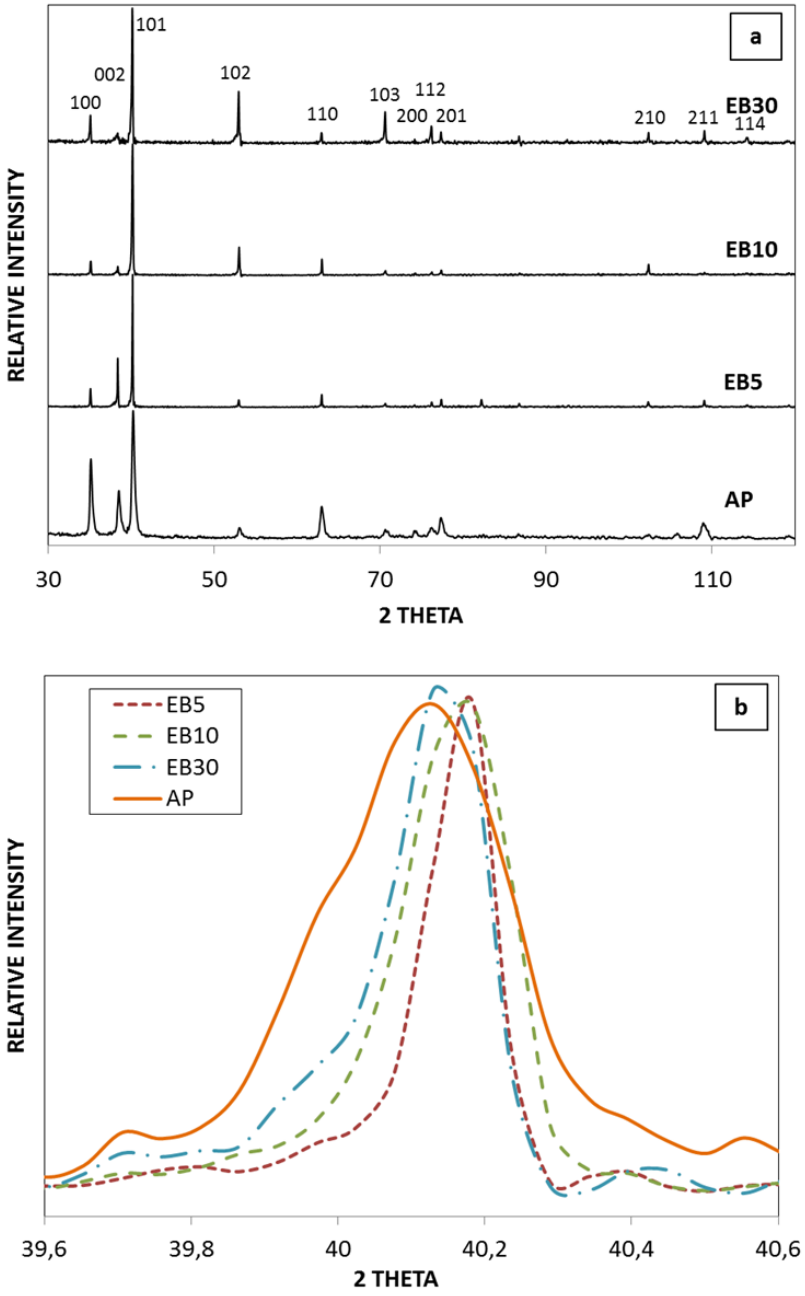

Figure 5: XRD spectra of the EB and AP samples: a) whole spectra, b) magnification of the main peak of α (101). All the spectra have been normalized to the highest peak.

All the spectra show the same peaks, which are attributable to α titanium with hexagonal crystal system (main peak at about 40.18°- (101) plane). The spectra of the mechanically roughened and EB surface structured samples have some small differences in the relative intensity of the peaks. The intensity of the diffraction peaks is proportional to the volume fraction of the elemental cells which expose the corresponding crystalline plane parallel to the surface and differences with respect to the random standard reference are related to the presence of a crystallographic texture. The AP sample has an increase of the intensity of the (100) peak, while the EB surface structured samples have some differences in the intensity of the (002) peak with respect to the random standard reference, even if no strong crystallographic texture can be registered on any sample. Concerning the position of the peaks, the 2θ location of the diffraction peak (101) is shifted to slightly higher 2θ values for the EB surface structured samples (mainly for the EB5 and EB10 samples) which denotes the presence of α' martensite, as reported by Gu et al (2012) for selective laser melting processed CP Ti.

The Full Width at Half Maximum (FWHM) of the highest peak is higher for the AP roughened sample (0.32°), compared to the EB structured ones (0.19° in the case of EB5 and EB10; 0.25° in the case of EB30), because the high temperature involved in EB structuring induces significant grain growth as observed by optical microscopy.

Residual stresses characterized by XRD are presented in Table 2, for the unstructured (mirror polished) and EB surface structured samples. The unstructured mirror polished sample can be considered a representative sample for both mirror polished and mechanically roughened samples considering that the second one was subjected just to an optimized surface polishing protocol. The mirror polished sample exhibited typical compressive stresses of mechanically polished surfaces (Axinte et al 2009), while, for the samples with grooves 5 and 10µm wide, tensile stresses were measured along the directions parallel (A) to the grooves. Significant compressive stress perpendicular (B) to the grooves is present in the sample with grooves 5 µm wide. In the case of the sample with grooves 30µm wide, practically negligible residual stresses were revealed. The observation of the tensile stresses are related to the molten zone during surface EB structuring (Robinson et al 1996) and the obtained values derive from the beam velocity (Maawad et al 2016) and consequently cooling rate during surface processing (Pfleging et al 2015).

Table 2. Residual stresses in two different positions of unstructured mechanically polished and electron beam structured surfaces.

Sample	Residual Stress	
	Direction A (parallel to groove)	Direction B (perpendicular to groove)
Unstructured (mirror polished)	-229±33MPa	
EB - 5µm gooves	138±13MPa	-130±54MPa
EB - 10µm gooves	164±35MPa	-9±39MPa
EB - 30µm gooves	88±13MPa	32±68MPa

It can be concluded from the physico-chemical characterization that EB surface structuring allows to get regular surface patterns with grooves 10 or 30 µm wide, but it introduces residual stresses, structural and microstructural changes too: all these features could potentially affect the biological response of the treated surfaces. Grooves 5 µm wide cannot be obtained because of the increment of roughness due to structure and microstructure changing.

3.2 Cellular tests

3.2.1 Cytompatibility evaluation

The results of cells viability are reported in Figure 6. In general, both direct (A) and indirect assay (B) did not report any significant differences between the surface structured (grooved) specimens and the bare titanium control (mirror polished titanium - $p>0.05$) after 48 h cultivation. Moreover, no statistically significant differences were noticed between data representative for different groove sizes ($p>0.05$).

In fact, results from both direct and indirect assays reported cells viability values >90% when normalized towards untreated controls (C). Accordingly, it can be speculated that the surface modifications made by EB technique (topography and microstructure) did not introduce any toxicity.

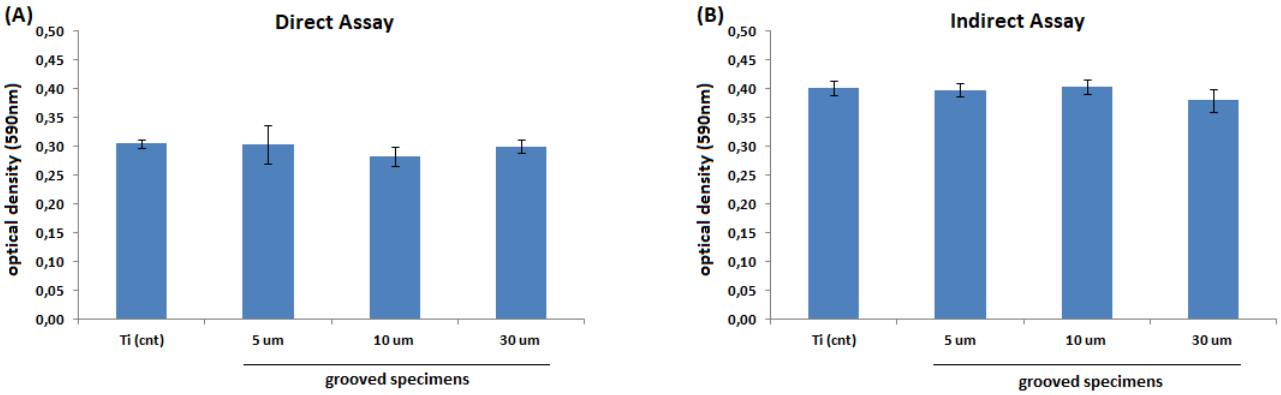

(C)

% Viability (vs Ti cnt)

grooved specimens	Direct Assay	Indirect Assay
5 um	99.5 (±10.8)	99.0 (±2.8)
10 um	92.5 (±5.8)	100.3 (±3.1)
30 um	98.3 (±3.8)	94.5 (±5.1)

Figure 6. Cytocompatibility evaluation. No statistically significant differences were noticed between the surface structured specimens and bare titanium (Ti cnt – mirror polished titanium) in terms of cells viability ($p>0.05$) for neither direct assay (A) nor indirect assay (B). No differences were noticed ($p>0.05$) between different grooved specimens. All the specimens showed viability values >90% in comparison with Ti cnt (C). Bars represent standard deviations.

3.2.2 Morphological analysis

FESEM observation of the EB - 5, EB - 10 and EB - 30 samples after 48h fibroblasts culture are reported in Figure 7, together with reference mirror polished (MP) and mechanically roughened (AP) samples.

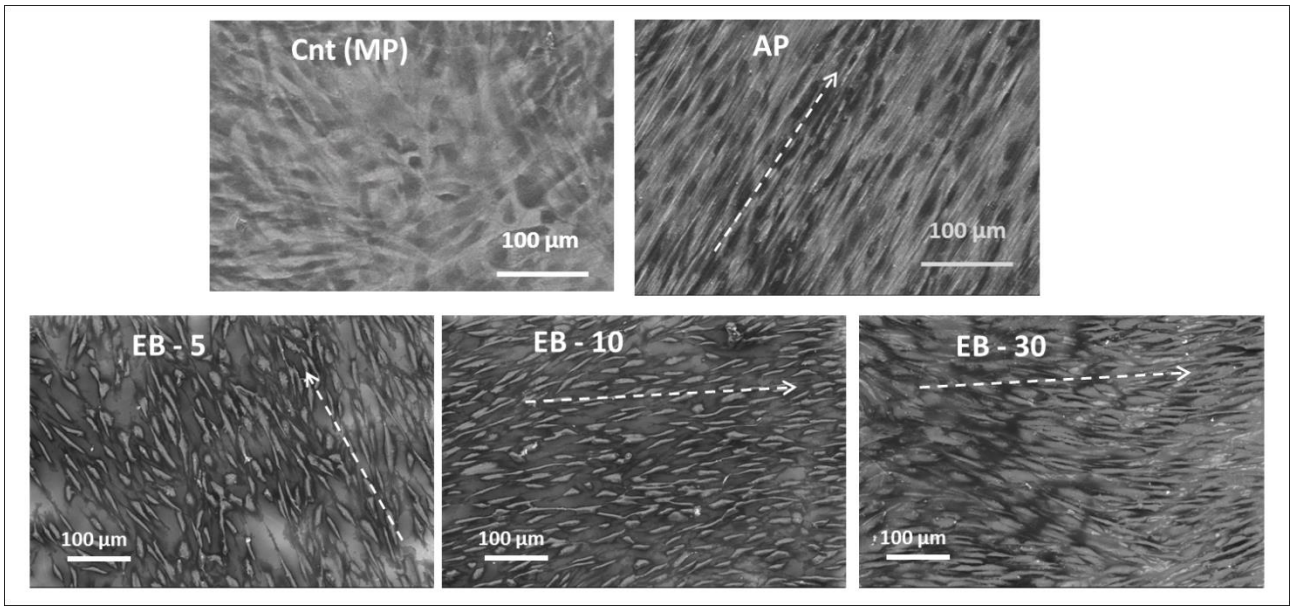

Figure 7: Representative FESEM images of reference mirror polished (MP) and mechanically roughened (AP) samples and EB surface structured ones after 48 cell culture. Arrows indicate grooves direction.

Multilayers of cells with different and crossing orientations can be observed on the mirror polished samples after 48h culture (Figure 7). Cells not well aligned and developed along different and locally crossing directions can be noticed on several areas of the EB-5 and EB-30 surfaces after 48h culture (Figure 7). On the other hand, all the cells follow the same direction on AP and EB-10 surfaces.

The different surface grooves size was noticed to influence cells spread and cytoskeleton orientation during the 48 h cultivation. In fact, as shown in Figure 8, cells follow the grooves orientation when their size is of 10 µm (B): this observation looks particular evident by checking actin filaments (stained in red with phalloidin) and vimentin (stained in green) staining.

On the opposite, only a moderate surface influence was noticed for 5 µm sized grooves where cells differed in terms of cytoskeleton orientation when random specimens regions were microscope investigated. Similarly, no surface influence was detected when cells were cultivated onto 30 µm sized grooves: cells cytoskeleton orientation was found to be randomly different onto different specimen areas.

The alignment of the cells, with respect to the grooves, and its statistical distribution was measured on the surface structured samples through image analysis, by using the images obtained through fluorescent microscope (phalloidin, Figure 8b). In the case of the sample with 10micron wide grooves, the average misalignment is 12°, the maximum misalignment (out of 50 measurements) is 28° and the standard deviation of the data is 8°, showing a good level of alignment of the cells. On the contrary, on the samples with grooves respectively 5 and 30 micron wide, no clear alignment was found (average misalignment respectively of 32 and 50° with a standard deviation of 24-38°). As reference, the orientation of the cells on the Ti-pol samples is in a range of 53° and the standard deviation of the data is 38°, showing an almost random distribution.

These results can be compared to what obtained on the mechanically roughened control (AP sample) where a strong alignment can be also obtained with a narrow and streamlined shape of the cells because of

the reduced width of the grooves with respect to the EB structured surfaces: the average misalignment is 5°, the maximum misalignment is 15° and the standard deviation of the data is 4.6°

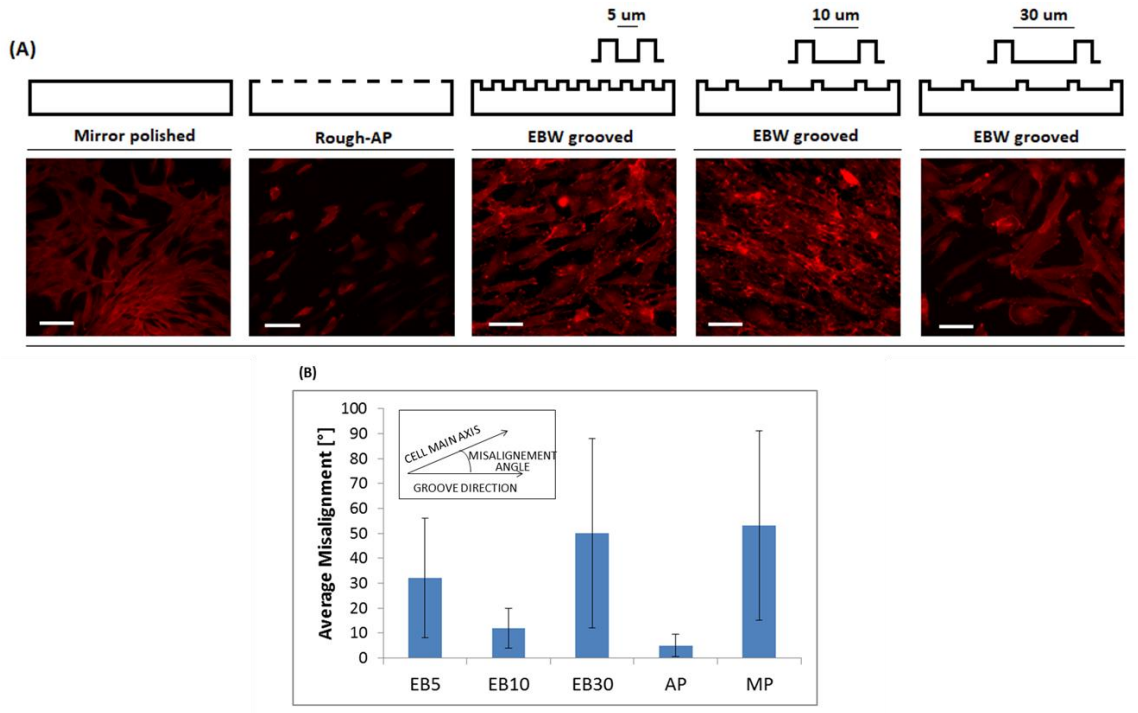

Figure 8. Surface grooves influence on cells cytoskeleton orientation. An evident effect was noticed when cells were cultivated onto 10 um sized grooves specimens as actin filaments (A, stained in red with phalloidin). A moderate grooves influence was noticed for 5 um sized grooves (A) while no effect was detected onto 30 um grooved surfaces (A) as cells were found to be randomly spread. Bar scale = 50 um, magnification 20x. The average misalignment angle of the cell main axis vs the groove direction is reported in (B)

The combination of electron beam structuring efficacy, cell dimension and ability to sense structures with similar dimension is at the basis of cell alignment. According to the obtained results, 5 µm grooves resulted not completely effective to stimulate fibroblast alignment, even if their spacing is compatible with cell sensing dimension. The issue related to 5 µm specimens is that they are not uniformly grooved and well developed and only some zones of the surface resulted as correctly grooved, as prior shown in Figure 1c. Consequently, their ability to affect fibroblast alignment is limited and only a moderate influence on the direction of fibroblast growth was detected. Differently, the 30 µm grooves spacing were homogeneously formed within the specimens' surface, thus resulting as effective in cells orientation. However, the 30 µm size probably resulted as larger than what required for cells ranging from 15 to 25 µm width, thus resulting in a partial guide for cells alignment.

Finally, looking at the data regarding 10 µm grooved specimens, they resulted into an optimal agreement between surface grooving (very homogeneous as prior showed in Figure 2d) and cells orientation (as demonstrated by IF images). These findings are in line to those reported by literature concerning different materials; for example, Gamboa et al. (2013) demonstrated that by using 10 µm spaced grooves onto PMMA substrates, it was possible to obtain a better cells alignment in comparison with 20 µm even if the grooves were realized by a wave-like not-linear topography. Same promising findings were described by

Agrawal et al. (2015): in fact, by using 10 µm width polycaprolactone fibres, they were successful in promoting smooth muscle cells alignment to promote new blood vessels formation.
A possible explanation of this behaviour was given by Zhou et al (2013); they demonstrated that cells alignment occurs after a sensible membrane deformation that can be due to the surface topography. Accordingly, the differences that we observed between 10 and 30 µm can be explained by the evidence that the 10 µm topography is certainly more stressing for cells spread than the 30 ones, thus resulting as more effective in forcing cells alignment. So, 10 µm grooved specimens were definitely considered as the most promising to satisfy the surface requirements debated in the work aims.

Then, the extracellular matrix (ECM) deposition was investigated by means of collagen deposition; results are reported in Figure 9. In general, no conspicuous differences were noticed between the specimens with different sized grooves. In fact, cells were able to correctly deposit collagen independently form the surface grooves size. Therefore, cells extracellular matrix (ECM) statement was not found to be related or influenced by the different size of specimens' surface grooves. However, as prior showed by vimentin staining, also collagen confirmed that cells were influenced by the presence of 10 µm grooves as also the ECM was deposited following the samples surface topography.

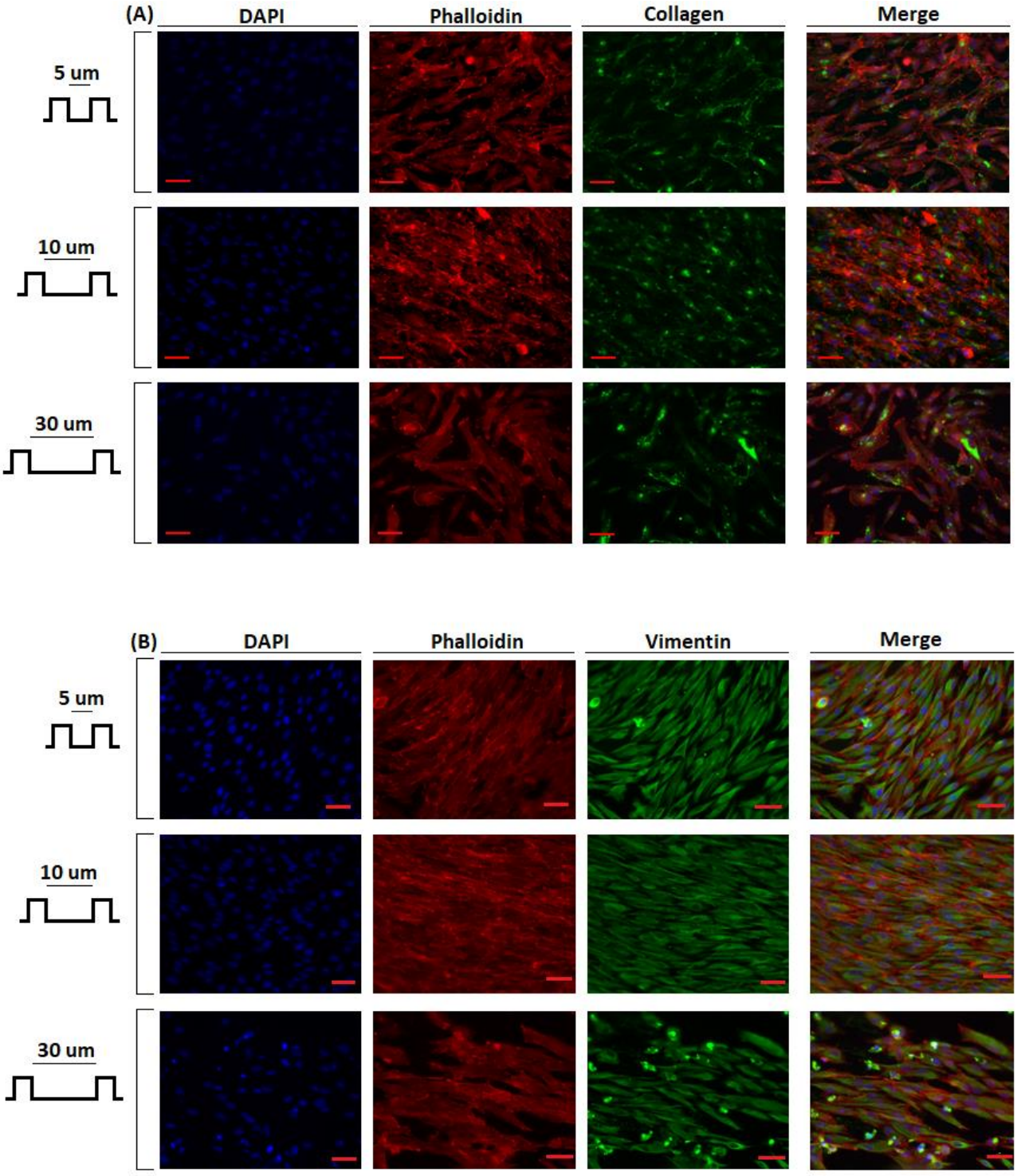

Figure 9. Cells matrix deposition onto EB surface structured (grooved) specimens. In general, HGFs were able to correct adhere and subsequently deposit collagen (A, stained in green) and Vimentin (B, stained in green) onto all different grooved specimens. Bar scale = 50 um, magnification 20x.

3.3 Bacterial adhesion

Results obtained by infecting mirror polished titanium control and EB surface structured specimens with *S. aureus* biofilm are reported in Figure 10. As expected, the EB surface structuring does not introduce any

increase in bacterial adhesion because surface roughness is below or just slightly higher (in the case of the 30 µm wide grooves) the threshold reported in literature at this respect. This is in agreement with what already observed by the authors in the case of the mechanically roughened surface, where at 48h a bacterial contamination statistically similar to the mirror polished surface was reported (Ferraris et al 2017). Actually, the results are beyond expectations and EB surface structuring introduced anti-adhesive properties to the specimens' surfaces that made difficult bacteria adhesion. In fact, after 2 h infection the viable biomass was lower on EB surface structured (grooved) specimens in comparison to the mirror polished controls (Figure 10A). Similar results were noticed at the following time-points (Figure 10B-C-D) where the EB surface structured specimens resulted as less contaminated. However, bacteria growth was fairly linear (Figure 10E) for all the specimens thus leading to the speculation that the EB surface structuring was not effective in cause bacteria death, but in decreasing the number of adherent bacteria in the first stage of the experiment. Accordingly, the CFUs count was assayed at the same time-points achieved for the alamar blue test. As expected, after 2 h infection the number of viable bacteria attached to the EB structured specimens' surfaces was about 2 logs lower than those observed onto controls (Figure 10F). Consequently, similar results were achieved in the following time-points (Figure 10G-H-I). However, also CFUs count assay confirmed that the number of viable bacteria increased in function of time (Figure 10J) thus confirming that the action introduced by EB surface structuring is actually related to the enhanced bacteria difficulty to adhere to the surface, in accordance with the absence of antibacterial agents able to effectively kill micro-organisms.

So, looking at these results, no correlation between the ability of reducing bacterial adhesion and the size of the grooves or the consequent presence of residual stresses on the surface can be speculated.

However, the appliance of the EBW procedure itself can lead to the formation of a peculiar combination of surface microstructure (grain growth as suggested by Sreekumari et al (2001) and to the consequent reduction of the density of grain boundaries as reported by Sreekumari et al (2005) for stainless steel), crystallographic structure (presence of martensite) and topography (nanoscale roughness due to martensite) for titanium surfaces (Puckett et al 2010) occurring on all the EB surface structured samples. On the opposite, that is not observable on the mechanically roughened surfaces neither on the mechanically polished ones. Further investigations will be carried on in order to separate and to discriminate the different effects of these surface features, and especially of microstructure, which is still poorly explored for titanium surfaces

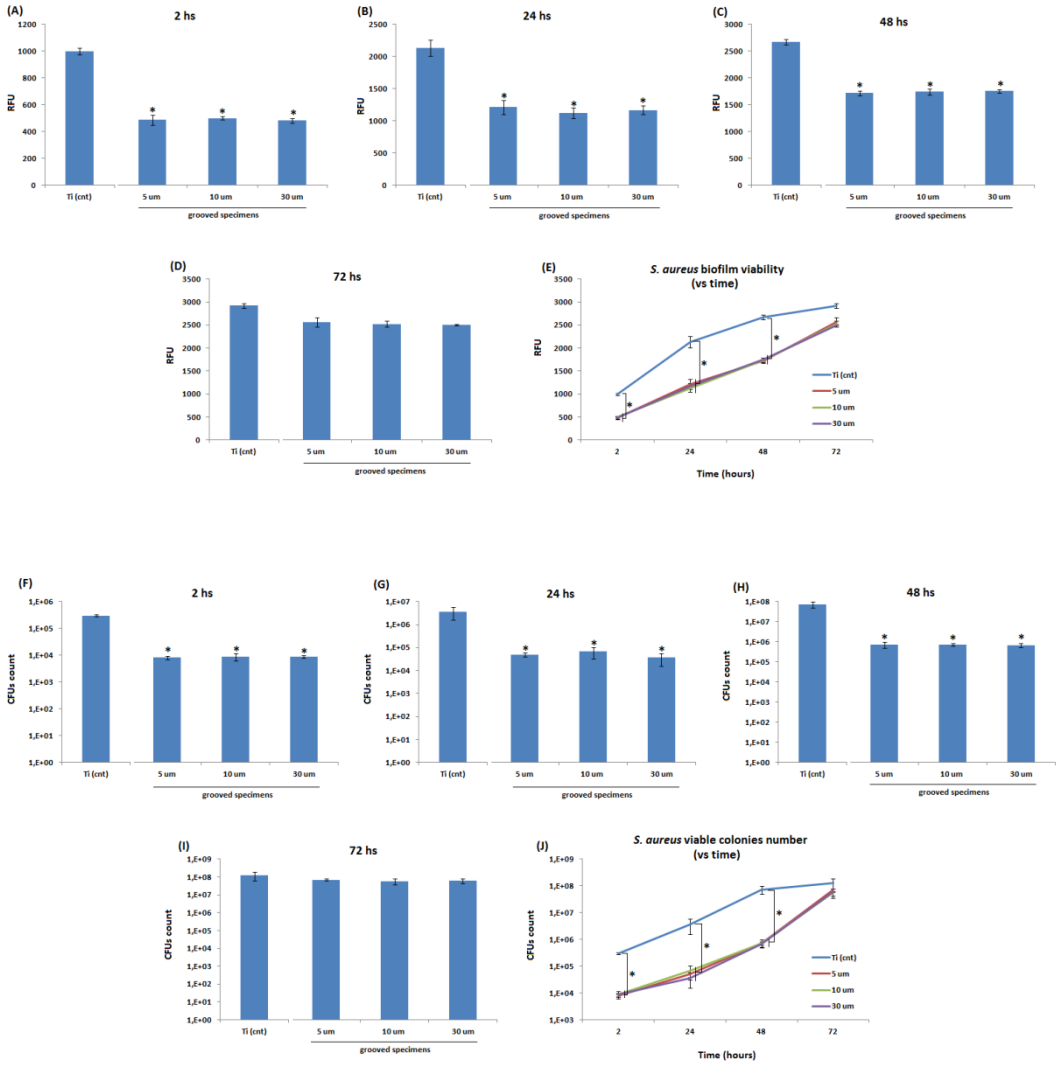

Figure 10. Bacterial adhesion. EB structuring introduced anti-bacteria adhesion properties to the specimens' surfaces. In fact, bacteria viable biomass was reduced onto EB grooved specimens in comparison with mirror polished titanium after 2hs (A); similar results have been noticed for the following time-points of 24 (B), 48 (C) and 72 (D) hs as summarized in (F). A possible explanation comes from attached colonies count: after 2hs the number of adhered bacteria was about 2 logs reduced onto the EB grooved specimens in comparison to the controls (F). Similar results were noticed in the subsequent time-points (G-H-I) confirming bacteria difficulty to colonize treated surfaces. Results are summarized in function of time in (J). Graphics represent means and standard deviations. *= $p<0.01$ groove vs cnt - one-way anova + Tukey post-hoc.

Conclusions

EB surface structuring is a promising technique in order to produce surface topographical patterns on the surface of c.p. Ti: parallel and regular grooves 10 or 30 µm wide can be obtained, which respectively are around 150 or 250 nm deep (peak to valley distance). EB surface topographical structuring of Ti is coupled with a consistent change in microstructure and crystallographic structure down to about 120 µm from the surface due to the thermal gradient during the EB process: grain growth and formation of α' martensite are observed and because of this regular 5µm wide grooves cannot be successfully achieved. Residual stresses are induced on the surface by the EB treatment and they are different for the different grooves dimensions.

Concerning the biological response of the EB surface structured samples, the strategy of using EB surface structuring in order to improve quality of soft tissues by contact guidance effect without an increased risk of bacterial contamination was confirmed by the results: 10 μm wide grooves have an influence on fibroblasts cytoskeleton orientation, with a strong alignment of the cells. A strong alignment can be obtained also by a proper mechanical surface structuring even if the geometry of the surface pattern is less regular and the cell shape is different from that of the EB samples because of the different groove width and spacing. Beyond the expected results, a reduction of bacterial adhesion in the first 48hs was observed on all the EB surface structured samples.

References

Agrawal, A.; Lee, B.H.; Irvine, S.A.; An, J.; Bhuthalingam, R.; Singh, V.; Low, K.Y.; Chua, C.K.; Venkatraman, S.S., 2015, Smooth Muscle Cell Alignment and Phenotype Control by Melt Spun Polycaprolactone Fibers for Seeding of Tissue Engineered Blood Vessels. Int J Biomater. 2015, 434876.

Al-Ahmad, A.; Wiedmann-Al-Ahmad, M. ; Fackler, A.; Follo, M.;Hellwig, E.; Bächle, M.; Hannig, C.; Han, J.-S.; Wolkewitz, M.; KohalR. 2013, *In vivo* study of the initial bacterial adhesion on different implant materials. Arch Oral Biol, 58, 1139-1147

Adam V., Clauß U., Dobeneck D. v., Thomas K., and Löwer T., 2011, in Elektronenstrahlschweißen Grundlagen einer faszinierdenden Technik, Pro-Beam A –Verlag, Germany.

Anselme K., Davidson P., Popa AM, Gizzon M., Liley M., Ploux L., 2010, The interaction of cells and bacteria with surfaces structured at the nanometer scale, Acta Biomaterialia 6, 3824-3846

Axinte D.A., Kwong J., Kong M.C., 2009, Workpiece surface integrity of Ti-6-4 heat-resistant alloy when employing different polishing methods, In J. Mater. Process. Technol., 209, 1843-1852

Brunette DM, 2001, Principles of cell behavior on titanium surfaces and their application to implanted device, in Titanium in Medicine, Springler-Verlag, Berlin Heidelberg New York, Chapter 15, pp 486-512

Dance A., BuxtonBGI , 2007, An Introductuion to Surfi-Sculpt Technology - New Opportunities, New Challenges, in *In Proceedings of the 7th International Conference on Beam Technology*, 2007, pp. 75–84.

Etheridge M. L., Campbell S. A., Erdman A. G., Haynes C. L., Wolf S. M., McCullough J. 2013, The big picture on nanomedicine: the state of investigational and approved nanomedicine products Nanomedicine9, 1-14

Ferraris S., Truffa Giachet F., Miola M., Bertone E., Varesano A., Vineis C., Cochis A., Sorrentino R., Rimondini L., Spriano S., 2017, Nanogrooves and keratin nanofibers on titanium surfaces aimed at driving gingival fibroblasts alignment and proliferation without increasing bacterial adhesion, Mat Sci Eng C 76, 1–12

Frijd, V.; Linderback, P.; Wennerberg, A.; de Paz, LC; Svensater, G.; Davies, JR 2011 Effect Of Nanoporous Tio2 Coating And Anodized Ca2+ Modification Of Titanium Surfaces On Early Microbial Biofilm Formation, BMC Oral Health, 11:8

Gamboa, J.R.; Mohandes, S.; Tran, P.L.; Slepian, M.J.; Yoon, J.Y., 2013, Linear fibroblast alignment on sinusoidal wave micropatterns. Colloids Surf B Biointerfaces. 104, 318-25.

Gu D., Hagedorn Y-C, Meiners W., Meng G., Santos Batista R., Wissenbach K., Poprawe R., 2012, Densification behavior, microstructure evolution, and wear performance of selective laser melting processed commercially pure titanium, Acta Mater 60, 3849-3860

Jaeger NAF, Brunette DM, 2001Production of microfabricated surfaces and their effect on cell behavior, in Titanium in Medicine, Springler-Verlag, Berlin Heidelberg New York;, Chapter 11, pp 344-374

Liu H., Webster TJ, 2007, Nanomedicine for implants: A review of studies and necessary experimental tools Biomaterials 28, 354-369

Liu H, Nakata K., Zhang J. X., Yamamoto N., Liao J., 2012, Microstructural evolution of fusion zone in laser beam welds of pure titanium, Mater. Charact. 65, 1–7

Lu X., Leng Y. 2005, Electrochemical micromachining of titanium surfaces for biomedical applications J. Mater. Process. Technol. 169, 173-178

Lütjering G., Williams J.C., 2003 in: Titanium Springer-Verlag Berlin Heidelberg New York.

Maawad E., Gan W., Hofmann M., Ventzke V., Riekehr S., Brokmeier H. G., Kashaev N., Müller M., 2016, Influence of crystallographic texture on the microstructure, tensile properties and residual stress state of laser-welded titanium joints, Mater Design 101, 137-145,

Madore C., Piotrowski O., Landolt D. 1999, Through-Mask Electrochemical Micromachining of Titanium J Electrochem Soc., 146, 2526-2526

Noyan I.C., Cohen J.B., 1987 Residual stress: measurement by diffraction and interpretation, Springer, 1987. http://dx.doi.org/10.1007/978-1-4613-9570-6

Oh M.S., Lee JY., Park J.K., 2004, Continuous cooling β-to-α transformation behaviors of extra-pure and commercially pure Ti, Mat Trans 35A, 3071-3077

Palanivel R., Dinaharan I., Laubscher R. F., 2017, Microstructure evolution and mechanical characterization of Nd:YAG laser beam welded titanium tubes, Mater. Charact. 134, 225–235

Pfleging W., Kumari R., Besser H., Scharnweber T., Majumdar J., 2015, Laser surface textured titanium alloy (Ti–6Al–4V): Part 1 – Surface characterization, Appl Surf Sci, 355, 104-111

Puckett S. D., Taylor E., Raimondo T., Webster T. J., 2010, The relationship between the nanostructure of titanium surfaces and bacterial attachment, Biomaterials 31, 706–713

Quirynen, M.; Bollen, CML; Papaioannou, W.; Van Eldere, J.;vanSteenberghe, D. 1996, The Influence Of Titanium Abutment Surface Roughness On Plaque Accumulation And Gingivitis: Short Term Observations, Int J Oral maxillofac Implants; 11, 69-178

Ramskogler C., Warchomicka F., Mostofi S., Weinberg A., Sommitsch C., 2017, Innovative surface modification of Ti6Al4V alloy by electron beam technique for biomedical application, Mat Sci Eng C 78, 105-113

Robinson J.M., Brussel B.A.V., Hosson J.T.M.D., Reed R.C., 1996, X-ray measurementof residual stresses in laser surface melted Ti–6Al–4V alloy, Mater. Sci. Eng. A208, 143–147.

Schultz, 2004, *Electron beam welding*. Abington Publishing Cambridge England,.

Spriano S., Ferraris S., 2014, How Can Topographical Surface Features Affect the Interaction of Implants with Soft Tissue?, in 3rd Int. Conf. On Health Science and Biomedical System HSBS14 Florence italy (22_24 Nov 2014)

Sreekumari K. R., Nandakumar K., Kikuchi Y. 2001, Bacterial attachment to stainless steel welds: Significance of substratum microstructure, Biofouling, 17, 303-316

Sreekumari K. R., Sato Y., Kikuchi Y. 2005, Antibacterial Metals: A Viable Solution for Bacterial Attachment and Microbiologically Influenced Corrosion, Mater Trans, 46, 1636 – 1645

Zhou, X.; Shi, J.; Hu, J.; Chen, Y., 2013, Cells cultured on microgrooves with or without surface coating: correlation between cell alignment, spreading and local membrane deformation. Mater Sci Eng C Mater Biol Appl. 33, 855-63.